Supersonic, Transverse Jet from a Rotating Ogive Cylinder in a Hypersonic Flow

D. L. McMaster* and J. S. Shang†
U. S. Air Force Aeronautical Laboratories, Wright-Patterson Air Force Base, Ohio
and
W. C. Golbitz‡
Defense Nuclear Agency, Washington, D.C.

Numerical simulations were performed for a supersonic jet issuing from a blunt-nosed ogive cylinder into a Mach 12 cross stream. All calculations employed the finite-differenced, mass-averaged Navier-Stokes equations with an algebraic eddy viscosity model for turbulence closure. One portion of the present investigation was focused on the numerical resolution requirement for the three-dimensional separated flowfield around the nonrotating body. The secondary separated flowfield structure was resolved with moderately increased grid density. The major portion of the present study was devoted to the simulation of the flowfield around the identical configuration, with the added complexity of rotating motion about the principal axis of the body. Numerical solutions over a wide range of angular velocities were obtained in the rotating frame of reference. At the low angular velocity of interest, the effects of body rotation on the flowfield structure were insignificant.

Nomenclature

D = diameter of jet aperture
e = total energy per unit mass
F,G,H = flux vectors defined by Eq. (1)
M = Mach number
P = pressure
P_t = pitot tube pressure
R = radius of cylinder
Rey = Reynolds number
r = radial distance from the axis of symmetry
S = rotational source vector defined by Eq. (2)
t = time
u = velocity vector
u,v,w = velocity components in the Cartesian frame
x,y,z = coordinates in the Cartesian frame
δ = boundary-layer thickness
ρ = fluid density
Ω = angular velocity, rad/s

Subscripts

i,j,k = unit vector in the Cartesian frame
j = condition of jet
0 = stagnation condition
∞ = freestream condition

Introduction

THE interaction of a transverse jet with an oncoming stream is a fundamental and important aerodynamic phenomenon in many flow regimes. In the subsonic domain, examples include the discharge of gases from smokestacks, mixing and combustion, and VTOL/STOL technology. For supersonic flows, the characteristics of the transverse jet interaction are important to control and maneuverability of aerospace vehicles, as well as to supersonic combustion. Our knowledge of this complex physical phenomenon is still very limited, however, and urgently needs continued research efforts.

Investigators have considered many aspects of the interacting transverse jet problem, including jet dynamics,[1-9] entrainment and mixing, [1-3,6,10] induced pressure distributions,[8,11,12] shock interactions,[8,11,13-15] and numerical solutions.[5-7,13,16] Few investigators have attempted to calculate the complete three-dimensional flowfield. Even fewer have attempted numerical simulations utilizing the ensembled compressible Navier-Stokes equations. None, to our knowledge, have studied the nature of the flowfield when the jet-issuing body is rotating with respect to its principal axis.

For the case of a supersonic primary stream and a nonrotating body, the flowfield is characterized by the inviscid/viscous interaction similar to that induced by a protuberance.[17,18] Complex patterns of shock interaction, together with three-dimensional vortical structures, are created as the flow is diverted around the jet. The phenomenon of interference that forms separation regions is well documented for many types of flowfield obstructions.[17,18] In the case of a jet in a hypersonic primary stream, the domain of influence is significantly reduced. Therefore, the gradients of flow properties are much steeper, and the scales of the resultant flow structures are changed. The three-dimensional separated flow must, however, obey topological rules that maintain the continuity of the flowfield.[17,19-21] In order to capture the detailed flowfield structure, a large amount of computing time is required.

When the jet-issuing body rotates about its longitudinal axis, there is no plane of symmetry to reduce the computational domain, and the grid resolution problem becomes more difficult. The first portion of the present study establishes the criterion for numerical resolution of the three-dimensional interaction generated by a supersonic jet issuing from a blunt-nosed ogive cylinder into a hypersonic stream.

The major portion of the present study concerns the calculation and correlation of the flowfield past the jet-issuing cylin-

Presented as Paper 87-1441 at the AIAA 19th Fluid Dynamics, Plasma Dynamics and Lasers Conference, Honolulu, HI, June 8-10, 1987; received Sept. 4, 1987; revision received March 10, 1988.

*Visiting Scientist. Member AIAA.
†Technical Manager. Associate Fellow AIAA.
‡Program Manager. Member AIAA.

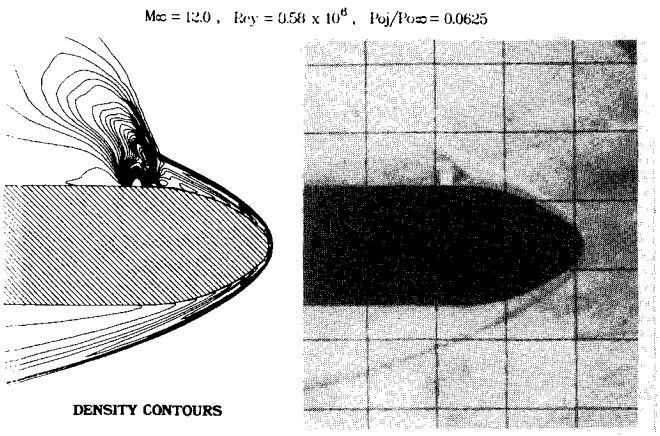

Fig. 1 Comparison of schlieren photograph with density contours for case A.

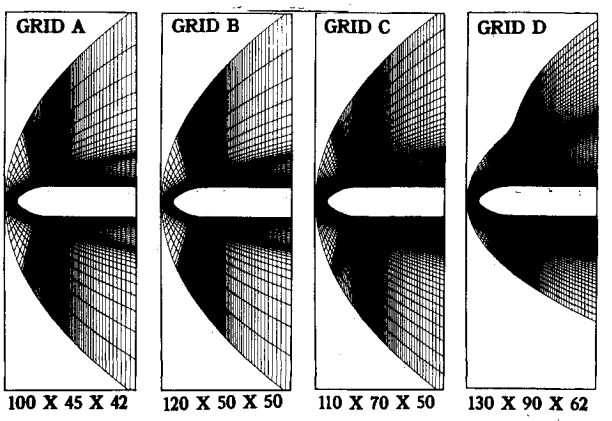

Fig. 3 Side view of grid points in the plane of symmetry.

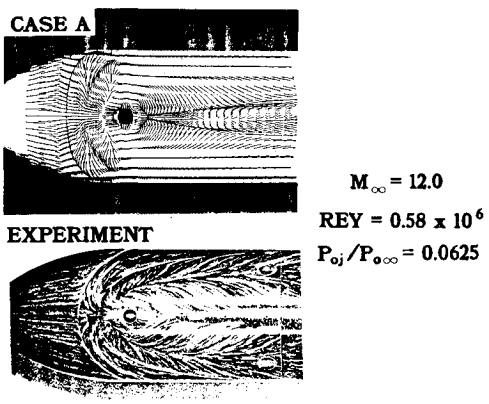

Fig. 2 Comparison of shear flow patterns.

der rotating about its longitudinal axis under identical test conditions. The numerical simulation is not dynamically coupled; the ogive cylinder is assumed to remain at zero angle of attack at all times. Two approaches are possible in describing the rotational fluid motion. The first method is to define the coordinates in the Newtonian frame and generate the instantaneous grid system according to the motion. The other approach is to describe the fluid motion in the rotating frame of reference.[22] This latter approach is more suitable to our present purpose. First, calculation in the rotating frame of reference is simpler because the grid need not be rotated at each time step. Second, because the deformation tensor is invariant under rotational transformation, calculation in the rotating frame of reference still allows us to determine viscous effects (such as the shear flow pattern) while maintaining an easily implemented computer code. Finally, the additional acceleration caused by the nonrectilinear motion can be singled out easily to assess the impact on the complete flowfield. Once the flowfield is obtained in the moving frame of reference, the results are compared to the nonrotating results to exhibit the change in the flowfield appearance from the viewpoint of a stationary observer. Of particular interest are 1) the global flow structure affected by the rotating motion, and 2) the flowfield properties in the jet plume.

Grid Refinement Study

Analysis

A side-by-side numerical and experimental study[13] of the entire flowfield for a configuration consisting of a transverse jet issuing from a blunt-nosed ogive cylinder was recently accomplished. This solution will be designated as case A. Figure 1 compares the schlieren photograph of the flow interaction with computed density contours. The global features of the flow are captured by the computation, although there is a slight discrepancy in the projected angle of the bow shock envelope induced by the jet. Based on our experience, this is a first clear indication of insufficient numerical resolution for this complex physical phenomenon. The shock structure can be determined but, as is common,[13,17,23] the profile is smeared because of the lack of grid-point density in the high-gradient region. We feel that the flowfield solution is still valid, but the shock smearing detracts from the value of the numerical simulation for this comparative study.

As a final representation of the accuracy of the computed solution, we examine Fig. 2, comparing the computed surface velocity vectors with photographic evidence from the experiment. Although the general agreement is reasonable, we can see a major topological discrepancy in the region upstream of the jet. The experimental oil pattern clearly shows two lines of convergence and two lines of divergence, which respectively indicate the lines of flow attachment and separation. The computed flowfield has only one clear line of convergence, and one line of divergence. This qualitative disparity represents a more serious topological problem in numerically replicating three-dimensional separated flows than does the previously described quantitative difference.

On the basis of the preceding observations, efforts were concentrated to determine the requisite grid refinement sufficient to negate the discrepancies noted between experimental and computational data. Particular emphasis was placed on the resolution of the separated flow upstream of the jet to achieve a grid invariant numerical solution. In the grid refinement process, we constructed the grid system by clustering grid points around the anticipated resultant shock wave envelope but without the explicit use of automated grid adaptation.

Four grids, designated grids A–D, were used for the resolution study. Side views of each grid are presented in Fig. 3. All grids had two regions of clustering in the normal direction. Grid points were clustered near the body to resolve the boundary layer and away from the body to capture the bow shock wave. The coarsest grid system, used in the previous study to calculate case A, had $100 \times 45 \times 42$ points in the streamwise, normal, and azimuthal directions, respectively. Grid B, which consisted of $120 \times 50 \times 50$ grid points, was designed to resolve the existence and location of the possible secondary vortical structure upstream of the jet. The results of computations on this grid are designated as case B. The additional 20 streamwise planes are added in the region upsteam of the jet. The streamwise spacing in this region is decreased by a factor of 2 over that of grid system A to order $\delta/10$, where δ is the undisturbed boundary-layer thickness computed at the jet location on the opposite side of the cylinder. The third grid, grid C, was generated in an attempt to capture the shock location downstream of the jet; it had $110 \times 70 \times 50$ points,

Table 1 Relative grid sizes

Case	Dimensions	Relative size[a]
A	$100 \times 45 \times 42$	1.
B	$120 \times 50 \times 50$	1.59
C	$110 \times 70 \times 50$	2.04
D	$130 \times 90 \times 62$	3.84

[a]Number of grid points/number of grid points for case A.

with the majority of the added points located downstream of the jet, between the body and the experimentally predicted shock location.

A fourth grid, D, was a final attempt to resolve as many of the features of the flowfield as possible in one grid system. Grid D represented increased spatial refinement over cases A–C, both upsteam and downstrem of the jet. It was dimensioned $130 \times 90 \times 62$ and was fitted to the general structure of the predicted shock wave envelope of jet interaction. The side view of this grid system shows that, downstream of the jet, the grid clustering for the anticipated shock wave envelope moves away from the body. The grid expansion is limited to the jet-injection side of the body; the opposite side retains the same basic spacing as the grids in cases A–C.

Table 1 compares cases A–D for their relative grid size, using case A as the baseline. Since computational time required to reach convergence is proportional to the number of grid points, one can see that the increase in resource consumption is significant for all three grid enhancements.

The numerical solutions were obtained using the three-dimensional, mass-averaged Navier-Stokes equations with a simple flux-gradient turbulence model.[24] The numeral procedure was based on MacCormack's explicit predictor-corrector algorithm,[25] vectorized for high-speed processors. The data processing rate was 4×10^{-5} s/grid point/iteration on the Cray 2 at NASA Ames Research Center. Local time stepping was used to speed convergence, with the required convergence criterion that the consecutive surface pressure change less than 1% over a characteristic time scale.

Discussion of Results

The comparison of computed pitot pressure profiles with increasing numerical resolution (cases A, C, and D), together with experimental data, is given in Fig. 4. In general, a steady improvement of shock wave definition was gained with higher grid-point density and better distribution of mesh nodes near the experimentally predicted location of the shock. Because the grid refinement of case B over that of case A is concentrated in the upsteam region of the jet, the difference between the two cases in computed pitot pressure profiles downsteam of the jet is negligible. For reasons of clarity, the results of case B are not included in the presentation. In particular, grid system D represented the most elaborate grid refinement and yielded the best agreement with data. The maximum deviation between experimental data and numerical results is persistently located at the wave front. In the cross-sectional plane opposite the strong jet interacting domain, equivalent to the flow over the ogive without mass injection, all numerical results, including the definition of the bow shock wave generated by different grid systems, are essentially identical. For the present analysis, numerical results indicate that a more detailed description of fine-scale fluid motion can be achieved by local grid refinement but does not significantly affect the overall flowfield structure.

Further refinement of the numerical results could be obtained by adding more grid points and by redistributing the mesh system at the expense of substantially more computing time. The use of shock-fitting or three-dimensional adaptive techniques conceivably might be even more effective in obtaining the desirable definition of the shock wave envelope. Finally, the influence of the turbulence model on the numerical

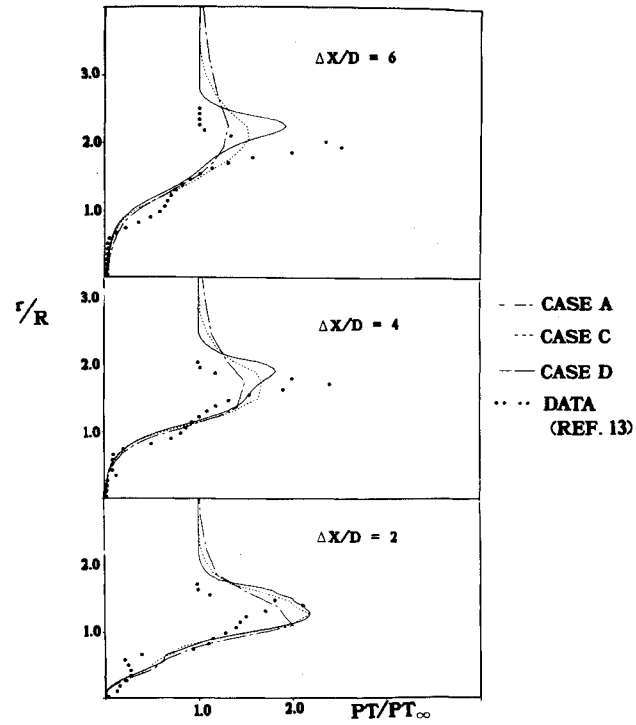

Fig. 4 Comparison of the pitot pressure profiles.

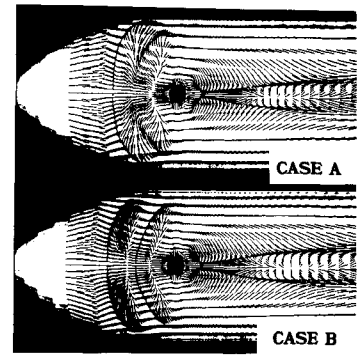

Fig. 5 Comparison of shear flow patterns.

results was evaluated by suppressing the numerical transition from laminar to turbulent flow downstream of the jet, thereby restricting the numerical simulation to laminar flow throughout the computational domain. This numerical result revealed a correct outward displacement of the shock wave structure downstream of the jet but did not demonstrate any significant change in the pitot pressure profile near the body surface.

The computed surface oil flow patterns are shown in Fig. 5 for cases A and B. The two numerical results are markedly different in that case B shows a distinct secondary convergence line near the plane of symmetry, whereas no such line is present in case A. In short, the resolution of case B enables capture of the detailed topological structure of the skin-friction line and the embedded multiple vortical formations of separated flow.[13,21] The locations of the lines of convergence and divergence are within the experimental error band of surface oil streaks under the identical flow conditions. This direct comparison suggests that the fully developed turbulent flow probably would not be encountered until downstream of jet. Therefore, in the present investigation, it is justified to assume that the flow remains laminar upstream of the jet.

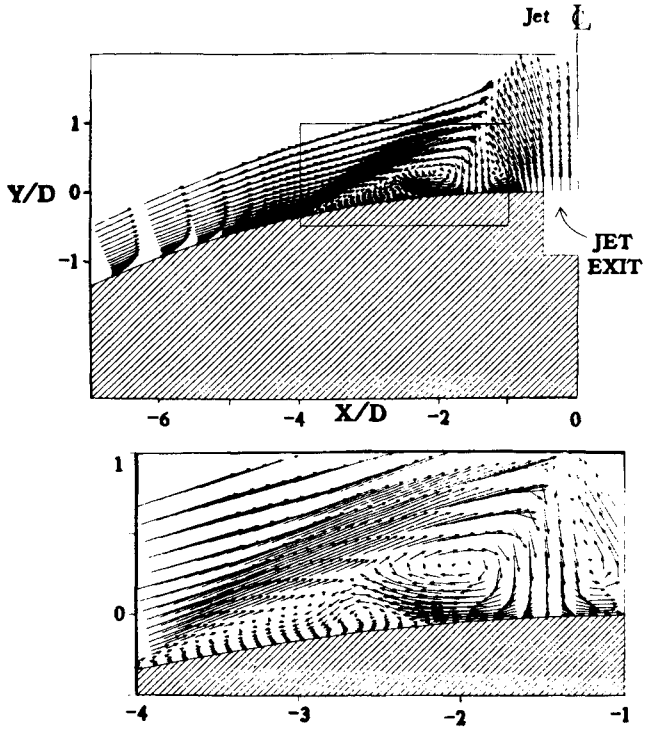

Fig. 6 Velocity vectors in the plane of symmetry.

A side view of the vector fields in the plane of symmetry ahead of the jet for case B is shown in Fig. 6. The velocity vectors indicate that the primary structure contains two counter-rotating vortices upstream of the jet, partitioned by the primary nodal point of attachment. Downstream of the nodal point and immediately upstream of the jet, the counterclockwise vortex is reinforced by the jet stream. Ahead of the attachment point, the fluid that originated far upstream and immediately adjacent to the surface spirals into the primary clockwise vortex at the saddle point. The next layer of fluid similarly forms the forwardmost secondary clockwise system. The rest of the entrained fluid develops into the secondary counterclockwise rotating vortex beneath the two clockwise vortices and appears as the secondary separated flow region. The greatest dimension associated with the secondary structure is less than the boundary-layer thickness of the unperturbed stream. The presence of the secondary separation region affected the global flowfield construct negligibly. Additional substantiation of this assertion also can be obtained by the identical density contours in the place of symmetry for cases A and B. Since the difference is undetectable, it is not included here. One may conclude that the increase in resolution for case B does increase the accuracy of the description of the separated flowfield. The predicted secondary vortical structure is found to replicate experimental observations. The secondary vortical structure influence is local, so that the relatively sparse resolution upstream of the jet is not critical in capturing the global nature of the flowfield.

The solutions for the surface shear pattern and the separated flow multiple vortical structures have not changed, even though the local grid refinement has been increased from case B to case D. The disparity between the two cases is minuscule, and the direct comparison is not repeated here. In essence, the locations of the primary convergence lines for both cases agree within $\delta/10$, and the remaining convergent and divergent limiting surface streamlines show even closer agreement. The overall structure of the shear pattern remains invariant upstream of the jet, with no new topological singularities observed. Thus, for this region, the solution is now grid-independent, and the solution of case B stands as representative of the complex interaction structure.

Rotation Study

Analysis

When the equation of fluid motion is expressed in the rotation frame of reference, the fictitious Coriolis and centrifugal forces must be explicitly included in the formulation. The Rossby number $U/L\Omega$, a convenient measure of the ratio of inertial and Coriolis forces, becomes an additional dynamic similarity parameter for rotating flow systems.[26] For a typical hypersonic aerodynamic configuration requiring spinning motion to maintain stability, the Rossby number is around 750. This Rossby number was simulated for the investigated configuration by rotation at an angular velocity Ω of 30 rad/s. The solution obtained at this Rossby number will be termed case E. In order to determine the influence of the Coriolis force on the pattern of the flowfield, solutions were also obtained at Rossby numbers of 75 (case F) and 7.5 (case G), spanning a range of three decades.

Grid A was chosen for the rotation study because it offered a reasonably accurate solution of global flowfield features at a minimum expenditure of computer resources. The numerical algorithm used for the rotation study was identical to the one used in the grid refinement study. When the Navier-Stokes equations are written in terms of the relative velocity in the rotating frame of reference, the basic form of the equations remains invariant.[22] The additional apparent Coriolis and centrifugal acceleration terms in the rotating frame are accounted for by adding source terms to four of the five equations. This is written in vector form as

$$\frac{\partial U}{\partial t}+\frac{\partial F}{\partial x}+\frac{\partial G}{\partial y}+\frac{\partial H}{\partial z}=S$$

where

$$\begin{aligned} S= &\ 0\\ = &\ -\rho[2\bar{\Omega}\times\bar{u}+\bar{\Omega}\times(\bar{\Omega}\times\bar{r})]\ i\text{th component}\\ = &\ -\rho[2\bar{\Omega}\times\bar{u}+\bar{\Omega}\times(\bar{\Omega}\times\bar{r})]\ j\text{th component}\\ &\ -\rho[2\bar{\Omega}\times\bar{u}+\bar{\Omega}\times(\bar{\Omega}\times\bar{r})]\ k\text{th component}\\ &\ -\rho\bar{u}\cdot[\bar{\Omega}\times(\bar{\Omega}\times\bar{r})] \end{aligned}$$

When the rotational motion is restricted about the streamwise axis of the body ($\bar{\Omega}=\Omega\bar{i}$), the source vector has only three nonzero terms:

$$\begin{aligned} S &= 0\\ &= 0\\ &= \rho\Omega^2 y+2\rho\Omega w\\ &= \rho\Omega^2 z-2\rho\Omega v\\ &= \rho\Omega^2(vy+wz) \end{aligned}$$

It may be interesting to note that the Coriolis force has no contribution to the energy equation, since it is a force directed at right angles to both the axis of rotation and the local velocity vector. The implementation of boundary conditions at the solid surface must also be changed in the rotating frame. The compatibility condition at the surface can be satisfied by changing the normal $\Delta P_{\text{wall}}=0$ to $\Delta P_{\text{wall}}=\rho\Omega^2 r\Delta r$, where ρ and r are evaluated at the body surface.

The relative impact of the Coriolis and centrifugal forces can be determined by computing and comparing their magnitudes throughout the flowfield. The centrifugal forces are linearly proportional to the radial distance from the axis of rotation, and their effect should become stronger in the outer region of the flow. The Coriolis forces, however, must reside where there are high velocity components normal to the axis of rotation. It follows that the strongest Coriolis force should occur as the jet issues from the body. Any small change in structure at this point should theoretically propagate and amplify downstream in the trajectory of the jet, so that the jet trajectory may serve as the best indicator of the presence of significant Coriolis effects.

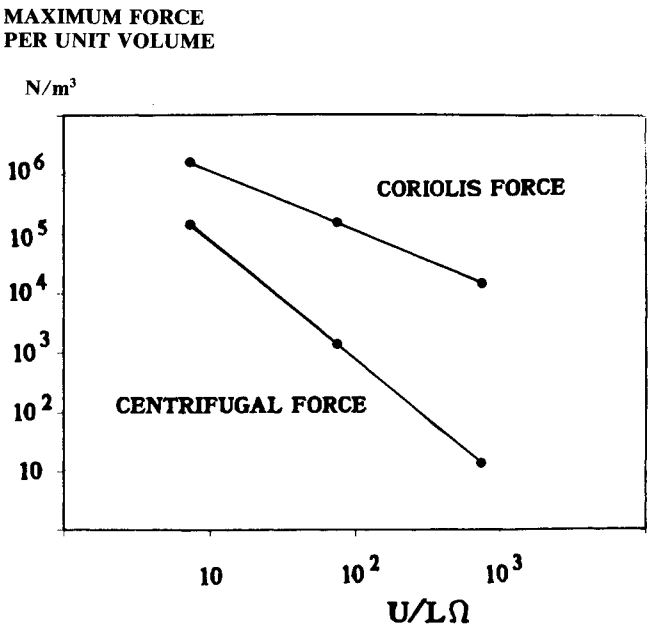

Fig. 7 Magnitude of maximum Coriolis and centrifugal forces vs Rossby number.

In the interaction region immediately upstream and downstream of the jet, velocities are small compared to other regions of the flowfield, especially those near the surface. The separated flow pattern is known to be sensitive to any small disturbances. One could expect that rotational forces might cause significant changes in the local structure. We will examine the local shear stress formations upstream and downstream of the jet for possible asymmetries.

Discussion of Results

Figure 7 depicts a comparison of the relative magnitude of the maximum Coriolis and centrifugal forces for cases E, F, and G. The centrifugal force is three orders of magnitude weaker than the Coriolis force for case E, the lowest spinning rate simulated. Even at an angular velocity 100 times greater than the case of interest, the centrifugal force, which is proportional to Ω^2, is an order of magnitude smaller than the Coriolis force. For all three cases studied, the centrifugal force probably has not substantially affected the formation of the flowfield.

Figure 8 consists of two contour plots that show the magnitude of the Coriolis force for sections of the entire flowfield for case E. In the longitudinal plane of symmetry, the Coriolis forces are shown to be strongest at the jet exit and negligible elsewhere. The contour levels exhibited in the figure represent the upper 90% values of the magnitudes of Coriolis force for the complete flowfield. The cross-sectional contours taken at the jet location again show that the Coriolis forces are significant only near the jet exit.

Figure 9 compares the cross-sectional view of the Mach number contours at the jet location for cases A, E, F, and G. One can see that case E, which satisfies the Rossby number similarity for a typical hypersonic configuration of practical interest, is identical to case A. Rotation at a rate 10 times higher than case E still yields no appreciable difference. It is only when the angular velocity is increased by two orders of magnitude over the rate of interest that a noticeable change in the shock structure takes place. In this case, the shock envelope immediately acquires an asymmetrical shape. The trajectory of the jet is disturbed only in case G, where it has already begun to shift away from the direction of rotation owing to the restoring effect of the Coriolis force.

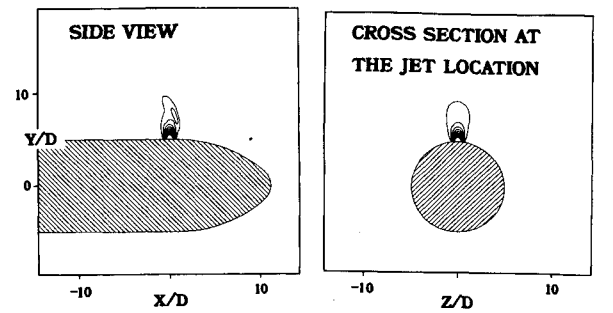

Fig. 8 Region of significant Coriolis forces, $U/L\Omega = 750$, $\Omega = 30$.

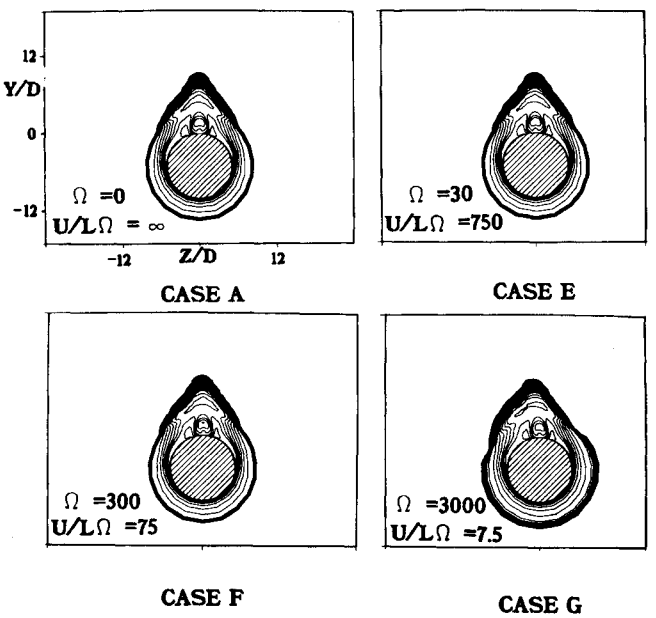

Fig. 9 Mach number contours, $X/D = 0$.

Downsteam of the jet, the effects of rotation are consistent with previous findings. Because the most pronounced rotational effects occur at the jet exit, the jet plume should accentuate disturbance. Figure 10, which presents Mach contours at a distance 12 jet diameters downstream of the jet, supports this observation. At the rotation rate that satisfies the similarity condition, no rotational effect can be observed on the flowfield. Only at the highest rotation rate computed is there an appreciable change in the shock structure and jet trajectory. For this case, the disturbance originates at the jet exit and propagates downstream.

The behavior of the shear vectors is identical for all four cases in the near-surface region upsteam of the jet. This is not surprising in view of the computed magnitude of Coriolis forces outlined earlier. In the separated flow region upstream of the jet, there are no rotation forces with sufficient strength to alter the flow. Results are slightly different downsteam of the jet. The surface shear patterns are the same for cases A, E, and F, but case G begins to show some asymmetry because of rotation. The footprint of the jet wake is shifted slightly away from the direction of rotation, which is consistent with the shift in both the jet trajectory and the shock structure.

The existence of significant changes in the flow properties near the jet can be determined by examining the close-up behavior of fluid density in that region. Figure 11 shows the cross-sectional contour of density at the jet location in detail for cases A, E, F, and G. The contours for cases A, E, and F are identical within the range of numerical error. Case G, simulating the highest rate of rotation, shows large changes of the local flowfield properties induced by the much higher rota-

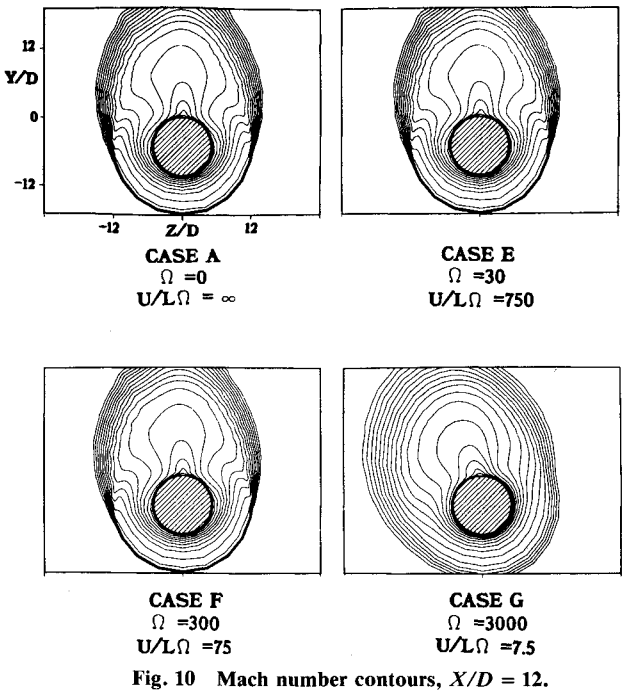

Fig. 10 Mach number contours, $X/D = 12$.

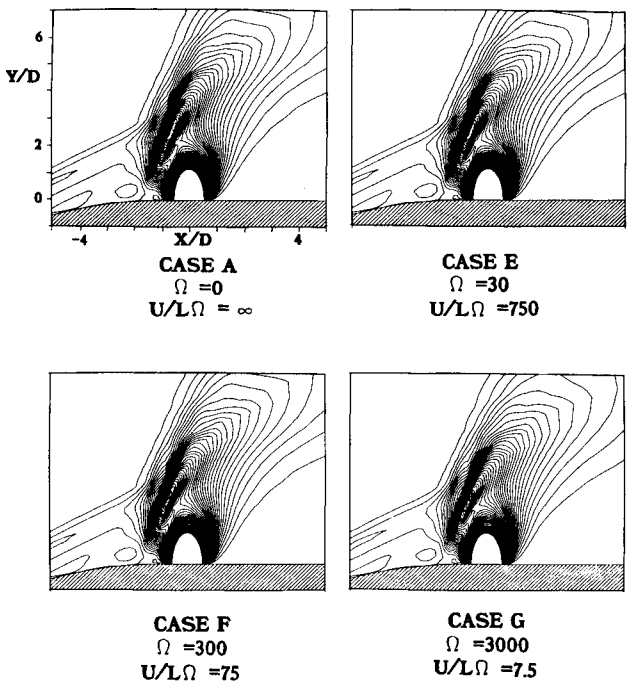

Fig. 12 Side view of density contours in the jet plane of symmetry.

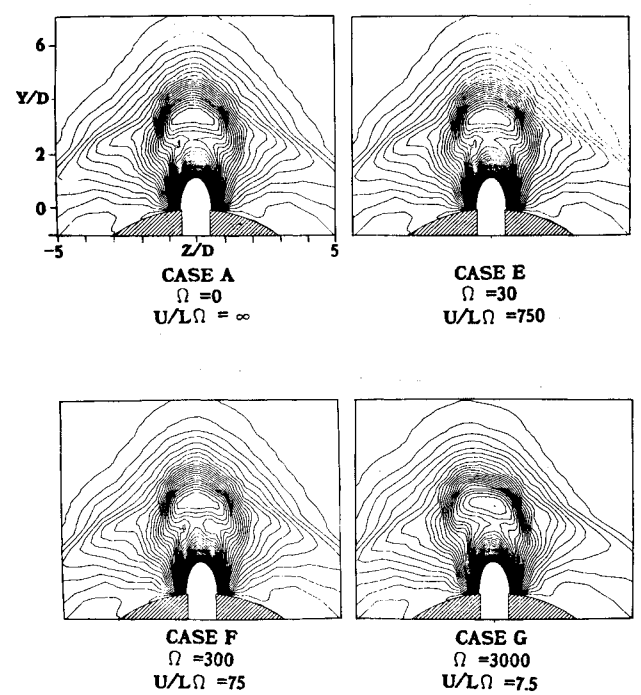

Fig. 11 Density contours at the jet cross section.

tion rate. The asymmetry of density contours in case G indicates a change in trajectory of the jet resulting from the Coriolis forces. Note, however, that very near the jet exit the density contours retain the symmetric distribution.

Figure 12 shows the side view of the plane of symmetry of the jet for cases A, E, F, and G. Here, no changes are noted in the flow properties near the jet for any of the computed results. This observation was anticipated and used as a benchmark for the present investigation. Because the centrifugal force is negligible in comparison with the Coriolis force and the latter must be directed at right angles to both the axis of rotation and the jet velocity, the rotational forces must be exerted only in the circumferential direction. The effect of rotation projected in the plane of symmetry of the jet is neither expected nor generated numerically for the cases unde consideration.

Conclusions

Flowfields of a supersonic jet ejected from an ogive cylinder into a hypersonic freestream with and without rotating motion have been numerically simulated. For the nonrotating calculations, the three-dimensional separated flow, consisting of two pairs of counter-rotating vortices, replicates experimental observations. Even though the definition of the resultant shock wave is smeared by the shock-capturing scheme, the computed complex vortical structure upsteam of the jet is accurate and independent of further mesh system refinement.

The rotating flow system was computed in a rotating frame of reference. Three different body rotation rates corresponding to a range of Rossby numers of 750, 75, and 7.5 were examined. At the highest Rossby number corresponding to the dynamic condition of practical engineering interest, the flowfield in the rotating frame of reference is identical to that in the nonrotating case. The entire flow formation rotates as a solid bulk. The jet plume and the downstream shock wave envelope exhibit a circumferential shift caused by the body rotation only at the lowest Rossby number examined, 7.5.

Acknowledgment

The computing resources provided by the NAS Systems Division, NASA Ames Research Center, are gratefully acknowledged.

References

[1]Keffer, J. F. and Baines, W. D., "The Round Turbulent Jet in a Cross-Wind," *Journal of Fluid Mechanics,* Vol. 15, 1963, pp. 481-496.

[2]Kamotani, Y. and Greber, I., "Experiments on a Turbulent Jet in a Cross Flow," *AIAA Journal,* Vol. 10, Nov. 1972, pp. 1425-1429.

[3]Adler, D. and Baron, A., "Prediction of a Three-Dimensional Circular Turbulent Jet in Crossflow," *AIAA Journal,* Vol. 17, Feb. 1979, pp. 168-174.

[4]Durando, N. A., "Vortices Induced in a Jet by a Subsonic Cross Flow," *AIAA Journal,* Vol. 9, Feb. 1971, pp. 325-327.

[5]Sykes, R. I., Lewellen, W. S., and Parker, S. F., "On the Vorticity Dynamics of a Turbulent Jet in a Crossflow," *Journal of Fluid Mechanics,* Vol. 168, 1986, pp. 393-413.

[6]Demuren, A. O., *Encyclopedia of Fluid Mechanics,* Vol. 2, edited by N. P. Cheremisinof, Blank Press, 1985, pp. 430-465.

[7]Chien, J. C. and Schetz, J. A., "Numerical Solution of the Three-Dimensional Navier-Stokes Equations with Application to Channel Flows and a Buoyant Jet in a Cross Flow," *Journal of Applied Mechanics,* Vol. 42, Sept. 1975, pp. 575-579.

[8]Zukoski, E. E. and Spaid, F. W., "Secondary Injection of Gases into a Supersonic Flow," *AIAA Journal,* Vol. 2, Oct. 1964, pp. 1689-1696.

[9]Manela, J. and Seginer, A., "Jet Penetration Height in Transonic Flow," *AIAA Journal,* Vol. 24, Jan. 1986, pp. 67-73.

[10]Broadwell, J. E. and Breidenthal, R. E., "Structure and Mixing of a Transverse Jet in Incompressible Flow," *Journal of Fluid Mechanics,* Vol. 148, 1984, pp. 405-412.

[11]Zubkov, A. I. and Glagolev, A. I., "The Effect of Boundary Layer Thickness and Transverse Curvature of the Surface on the Geometry and Forces Acting in the Separation Zone Produced by Injection of a Jet into a Supersonic Flow Over That Surface," *Fluid Mechanics—Soviet Research,* Vol. 8, Jan.-Feb. 1979, pp. 69-79.

[12]McMahon, H. M. and Mosher, D. K., "Experimental Investigation of Pressures Induced on a Flat Plate by a Jet Issuing into a Subsonic Crosswind," NASA SP-218, Paper 4, 1969.

[13]Shang, J. S., McMaster, D. L., Scaggs, N., and Buck, M., "Interaction of Jet in Hypersonic Cross Stream," AIAA Paper 87-0055, Jan. 1987.

[14]Avduevskii, V. S., Medvedev, K. I., and Polyanskii, M. N., "Interaction of a Supersonic Flow with a Transverse Jet Injected Through a Circular Aperture in a Plate," *Izvestiya Akademii Nauk SSSR, Mekhanika Zhidkosti i Gaz,* No. 5, 1970, pp. 193-197.

[15]Glagolev, A. I., Zubkov, A. I., and Panov, Yu. A., "Supersonic Flow Past a Gas Jet Obstacle Emerging from a Plate," *Izvestiya Akademii Nauk SSSR, Mekhanika Zhidkostii Gaza,* No. 3, 1967, pp. 97-102.

[16]Baker, A. J., Snyder, P. K., and Orzechowski, J. A., "Three Dimensional Nearfield Characterization of a VSTOL Jet in Turbulent Crossflow," AIAA Paper 87-0051, Jan. 1987.

[17]Peake, D. J. and Tobak, M., "Three-Dimensional Interactions and Vortical Flows with Emphasis on High Speeds," AGARD-AGA-252, July 1980.

[18]Settles, G. S. and Dolling, D. S., "Swept Shock Wave/Boundary-Layer Interactions," *Progress in Astronautics and Aeronautics: Tactical Missile Aerodynamics,* Vol. 104, edited by M. Hemsch and J. Nielsen, AIAA, New York, 1986.

[19]Lighthill, M. J., *Laminar Boundary Layers*, edited by L. Rosenhead, Oxford Univ. Press, New York, 1963, pp. 72-82.

[20]Hunt, J. C. R., Abell, C. J., Peterka, J. A., and Woo, H.,"Kinematical Studies of the Flows Around Free or Surface-Mounted Obstacles; Applying Topology to Flow Visualization," *Journal of Fluid Mechanics,* Vol. 86, 1978, pp. 179-200.

[21]Tobak, M. and Peake, D. J., "Topology of Three-Dimensional Separated Flows," *Annual Review of Fluid Mechanics,* 1982, pp. 61-85.

[22]Linton, S. W. and Shang, J. S., "A Numerical Simulation of Jet Impingement Cooling in a Rotating Frame of Reference," AIAA Paper 87-0609, Jan. 1987.

[23]Hung, C.-M. and Buning, P. G., "Simulation of Blunt-Fin-Induced Shock-Wave and Turbulent Boundary-Layer Interaction," *Journal of Fluid Mechanics,* Vol. 154, 1985, pp. 163-185.

[24]Baldwin, B. and Lomax, H., "Thin Layer Approximation and Algebraic Model for Separated Turbulent Flows," AIAA Paper 78-257, Jan. 1978.

[25]MacCormack, R. W., "The Effect of Viscosity in Hypervelocity Impact Cratering," AIAA Paper 69-354, Jan. 1969.

[26]Batchelor, G. K., *An Introduction to Fluid Dynamics,* Cambridge Univ. Press, 1967, pp. 555-557.